Journal of Materials Chemistry A

Accepted Manuscript

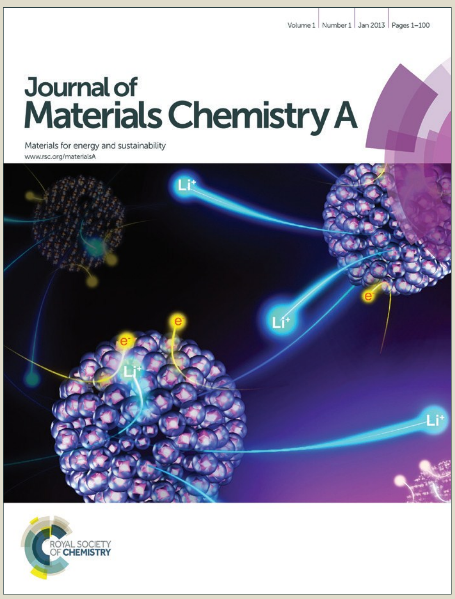

Journal Name

RSCPublishing

ARTICLE

Bifunctional TiO_2 Underlayer for α–Fe_2O_3 Nanorod based Photoelectrochemical Cells: Enhanced Interface and Ti^{4+} Doping

Cite this: DOI: 10.1039/x0xx00000x

Received 00th January 2012,
Accepted 00th January 2012

DOI: 10.1039/x0xx00000x

www.rsc.org/

Alagappan Annamalai[a], Pravin S Shinde[a,b], Arunprabaharan Subramanian[a], Jae Young Kim[b], Jin Hyun Kim[b], Sun Hee Choi[c], Jae Sung Lee[b] and Jum Suk Jang[a*]

A thin, compact TiO_2 underlayer for hematite-based photoelectrochemical cells was prepared by simple spin coating and showed a dramatic increase in device performance and photocurrent density. The introduction of TiO_2 underlayers induced a noticeable change in nanostructure. In contrast to the conventional strategies based on underlayers, the compact TiO_2 underlayers can both act as a charge recombination barrier and also as a source for titanium dopants. One could simply take advantage of fortuitous doping of Sn from FTO into hematite lattice during the activation step, and is converted into intentional doping of Ti^{4+} from the TiO_2 underlayer into the hematite lattice. Ti^{4+} doping in hematite lattice is highly probable during sintering of FTO/TiO_2/α–Fe_2O_3 photoanodes at 800°C, which has been confirmed by XPS measurements. Based on electrochemical studies, it is evident that the TiO_2 underlayer effectively suppresses charge recombination at the FTO/α–Fe_2O_3 interface and provides possible Ti^{4+} doping apart from Sn diffusion from FTO substrates when sintered at high temperatures (800°C). In contrast, only charge recombination was suppressed at lower sintering temperatures (550°C). This is the first report on elemental doping of Ti^{4+} from the TiO_2 underlayer when sintered at high temperature.

Introduction

Hematite (α–Fe_2O_3) is a promising candidate as a semiconductor photoanode for photoelectrochemical (PEC) water splitting due to its favorable band gap (2.2 eV), extraordinary chemical stability and abundance.[1-3] However, hematite photoanodes suffer from short hole diffusion length and extremely poor conductivity, which are some of the major drawbacks yet to be overcome.[4] One-dimensional (1-D) nanostructures of hematite have shown significantly improved photocurrent densities and can reduce the diffusion problem.[5]

Charge recombination is another common issue in PECs that limits the device performance.[6] Recombination takes place mainly at the transparent conducting oxide (TCO)/electrolyte and TCO/photoanode interfaces.[7] It is widely speculated that a dead layer exists near the TCO/photoanode interface, which has a detrimental effect on device performance.[8] A way to prevent this is by applying a metal oxide layer (blocking layer) on the FTO surface before the hematite photoanode.[9,10] This so-called blocking layer physically blocks the reaction of the photoinjected electrons at the FTO/α–Fe_2O_3 interface.

The blocking layer concept is attractive not only for PECs, but also in the area of dye sensitized solar cells (DSSCs), where metal oxide thin films successfully prevent charge recombination.[11] Suitable metal oxide semiconductors selected as effective blocking layers must have a low resistivity, a high work function, proper band alignment, and high transparency. Ultra-thin underlayers of Nb_2O_5[9], SiO_2[9, 10], Ga_2O_3[12], ATO[13], and TiO_2[9,14] have been reported only for ultrathin hematite photoanodes. The principle behind these ultrathin blocking layers is to block charge recombination at the FTO/hematite interface, and thus improve the water splitting efficiency.[9] Among the above-mentioned semiconductor metal oxides, TiO_2 is the most suitable candidate as a blocking layer and has been investigated most frequently in the case of DSSCs.[15] Besides the blocking effect, a higher density of TiO_2, together with a larger contact area and improved adherence between the TiO_2 layer and FTO surface provides better electron pathways from the hematite to FTO substrates, which facilitates electron transfer and subsequently improves the electron transfer and charge collection efficiency.[13]

Ultra-thin underlayers have been reported only for ultrathin hematite photoanodes since extremely thin (10–40 nm) hematite absorbers are used to minimize charge recombination due to the short diffusion lengths of photoexcited charge carriers.[5] In this paper, we demonstrate enhanced photocurrent efficiency with a TiO_2 underlayer for 400-nm α–Fe_2O_3 nanorod array-type photoanodes, as Ga_2O_3 underlayers did not show any improvement in PEC properties of 700-nm thick hematite photoanodes.[12] TiO_2 underlayers on FTO substrates were prepared by a simple spin coating method. Spin coating is simple and complementary to atomic layer deposition (ALD), since it does not require a complicated, high vacuum, and expensive system and it is easy to apply for any type of compact metal oxide blocking layers. Enhanced performance in hematite photoanodes (even at low sintering temperature) were observed when TiO_2 blocking layers were introduced between the FTO substrate and hematite nanostructures. To the best of our knowledge, none of these underlayers have been investigated for other types of photoanodes other than ultrathin hematite photoanodes; furthermore, none have been treated with high temperature sintering to induce elemental doping from the underlayer. The performance enhancement is attributed mainly to improved interfacial properties at the FTO/TiO_2/α–Fe_2O_3 interface and possible Ti^{4+} doping taking place from the TiO_2 underlayer not associated with Sn diffusion from FTO substrates when sintered at high temperature (800°C). In the following, the hematite photoanodes with a TiO_2 underlayer are designated as FTO/TiO_2/α–Fe_2O_3, and those without a TiO_2 underlayer are designated as FTO/α–Fe_2O_3.

Experimental Section

Preparation of TiO_2 Underlayers.

Fluorine-doped tin oxide (FTO) glasses (2.2 mm thick, 8 Ω /sq) were cleaned with distilled water and ethanol. For a compact TiO_2 underlayer the cleaned FTO glasses were coated with titanium diisopropoxide bis(acetylacetonate) solution by the spin-coating (1500 rpm for 30 sec), which was then heated at 250°C for 30 min.

Hydrothermal Synthesis of α–Fe_2O_3 Photoanodes.

Hematite nanorods on FTO glass and TiO_2 modified FTO glass were prepared by a simple hydrothermal method as reported by Vayssieres et al.[16] In a typical experiment, a piece of cleaned FTO glass was placed within a vial containing a solution consisting of 0.4 g $FeCl_3$•6H_2O and 0.85 g $NaNO_3$ at pH 1.5 (adjusted by HCl). The hydrothermal reaction was conducted at 100°C for 6 h. After cooling down to room temperature, the FTO glass was rinsed several times with distilled water and then dried at 60°C. Annealing at 550°C for 4 h was carried out for the phase transition from β–FeOOH to pure α–Fe_2O_3. Then the 550°C sintered samples were subjected to high temperature sintering.

Characterization

X-ray diffraction (XRD) patterns of all the samples were collected using an X-ray diffactometer (Rigaku RINT 2500) with CuKα radiation. The surface morphology of the samples was analyzed using field emission scanning electron microscopy (FESEM, JEOL JSM 700F). The oxidation states of dopants were studied using X-ray photoelectron spectroscopy (EscaLab 220-IXL, VG Scientific, monochromated Al Kα). The thickness of TiO_2 underlayer films was measured using a spectroscopic ellipsometer (J. A. Woollam Co. M-2000). HR-[S]TEM, Jeol, JEM 2200FS, 200 kV) with electron energy loss spectroscopy (EELS) mapping capabilities has been used to study the elemental doping of Sn and Ti at the National Center for Nanomaterials Technology, Postech, Korea. X-ray absorption fine structure (XAFS) measurements were conducted to investigate local structures of Fe_2O_3 photoanodes on 7D beamline of Pohang Accelerator Laboratory (PLS-II, 3.0GeV0, Korea). The incident beam was monochromatized using a Si(111) double crystal monochromators and detuned by 30% to minimizer higher harmonics. The spectra for K-edges of Fe (E_0=7112 eV) were taken in a fluorescence mode at room temperature under helium atmosphere. The obtained data were analysed with Athena in the IFEFFIT 1.2.11 suite of software programs.[17]

Photoelectrochemical measurements

All photoelectrochemical measurements were carried out in 1M NaOH (pH=13.8) electrolyte using Ivium compactstat potentiostat with a Platinum coil as counter electrode and Ag/AgCl as reference electrode. Photocurrent-potential (J-V) curves were swept at 50 mVs^{-1} from -0.7 to +0.7 *vs*. Ag/AgCl. For measuring the incident photon-to-current conversion efficiencies (IPCE), a 300 W xenon lamp (Newport, 6258) was coupled to a grating monochromator (Newport, 74125) operating in the wavelength range from 330 to 600 nm, and the incident light intensity was measured with a UV silicon detector (Newport, 71675). The photoelectrode was biased at +0.6 or +1.0 V (*vs*. Ag/AgCl) during all IPCE measurements. Impedance spectroscopy measurements were performed using an impedance analyzer (Ivumstat). The impedance spectra were measured over a frequency range of 1×10^{-2} to 3×10^{6} Hz at 25°C under open circuit conditions with amplitude of 10 mV and under a bias illumination of 100 mW cm^{-2}.

Results and discussion

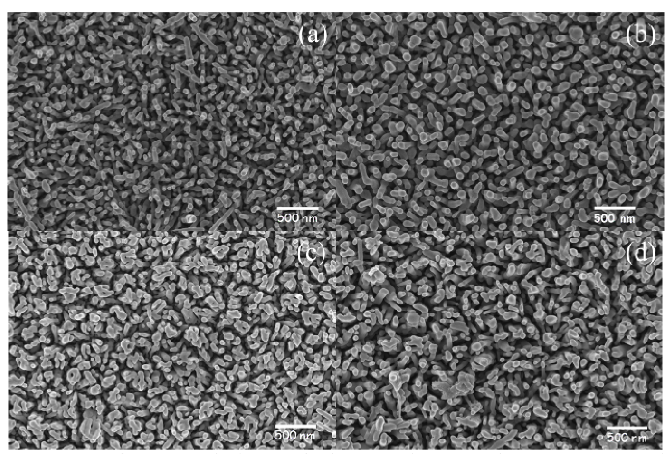

Fig. 1. Surface morphology of photoanodes: FTO/α–Fe_2O_3 nanorods sintered at (a) 550°C, (b) 800°C, and FTO/TiO_2/α–Fe_2O_3 nanorods sintered at (c) 550°C and (d) 800°C.

Fig. 1 (FESEM images) depicts the morphology of hematite nanostructures on a TiO_2 underlayer that is distinct from that grown on bare FTO substrates. The FTO/α–Fe_2O_3 photoanodes in Figs. 1a and 1b possesses a similar morphology to that of previous reports.[18] A noticeable change in nanostructure was observed when a compact TiO_2 underlayer was introduced between the FTO substrate and α–Fe_2O_3 nanostructures. FTO/TiO_2/α–Fe_2O_3 photoanodes consist of irregular clusters and possess a similar morphology to that of FTO/α–Fe_2O_3 photoanodes, shown in Figs. 1c and 1d. The distinct morphology of FTO/TiO_2/α–Fe_2O_3 photoanodes originates from the inclusion of the TiO_2 underlayer. The Gibbs adsorption isotherm states that any adsorption phenomenon at the water – oxide interface will decrease the surface tension for nucleation and growth in an aqueous solution.[19, 20] Thus, it is reasonable that the morphology and orientation of FTO/TiO_2/α–Fe_2O_3 photoanodes depends on growth conditions that are expected to change upon introduction of TiO_2 underlayers. The considerable difference in the FTO/TiO_2/α–Fe_2O_3 morphology, induced by the TiO_2 underlayer, can be explained by a different nucleation and growth process. No diffraction peaks of Ti or other impurity phases other than α–Fe_2O_3 were observed in both FTO/α–Fe_2O_3 and FTO/TiO_2/α–Fe_2O_3 photoanodes, as shown in Fig. S1 †.

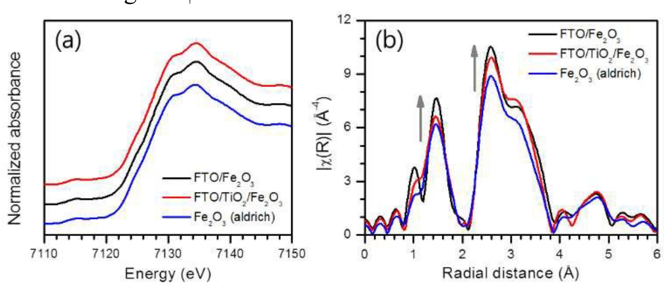

Fig. 2. (a) Fe K-edge XANES spectra and (b) Fourier-transforms of Fe K-edge EXAFS for FTO/α–Fe_2O_3 and FTO/TiO_2/α–Fe_2O_3 photoanodes and reference Fe_2O_3 powder.

Local electronic structures around the Fe atom are all the same, but more ordering is observed for FTO/α–Fe_2O_3, which is in accordance with the morphology characteristics, as shown in Fig. 2. While the electronic structure was examined with Fe K-edge XANES (X-ray absorption near-edge structure) spectra, the geometrical structure depicting neighboring environment around a central Fe atom could be explored by analyzing the Fe K-edge EXAFS (Extended x-ray absorption fine structure) data. In the Fourier transformed data, the increase in the intensities of the first and the second peaks directly correlates with decreasing the Debye-Waller factor because the coordination numbers of Fe-O (1st shell) and Fe-Fe & Fe-O (2nd shell) are invariant. The Debye-Waller factor, indication of structural disorder, decreases in the sequence of Fe_2O_3 (powder) > FTO/TiO_2/Fe_2O_3 > FTO/Fe_2O_3. The materials with lower Debye-Waller factors represents a well ordered atomic structure/arrangement. We observed an increase in Debye-Waller factor for FTO/TiO_2/Fe_2O_3 photoanodes, which might be due to an increase of static disordering resulting from the TiO_2 underlayer.

The absence of any indication of Ti or additional peaks in the XRD spectrum and the lack of differences in the Fe K-edge XANES spectra imply that the modifications due to TiO_2 underlayers are limited to the FTO/α–Fe_2O_3 interface. The presence of a TiO_2 layer on the surface of FTO substrates was confirmed by UV-vis spectroscopy, as shown in Fig. S2(a) †. Images derived from TEM and EDS mapping of the hematite showed the presence of Ti across the FTO/α–Fe_2O_3 interface region (see Fig. S3 †). This is further evidence of the formation of a TiO_2 underlayer at the FTO/α–Fe_2O_3 interface.

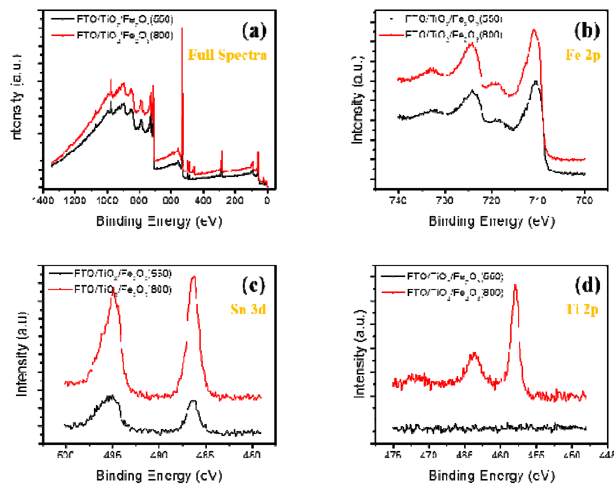

Fig. 3. X-ray photoelectron spectra of (a) full scan, (b) Fe 2p, (c) Sn 3d, and (d) Ti 2p recorded from 550°C and 800°C sintered FTO/TiO_2/α–Fe_2O_3 photoanodes.

X-ray photoelectron spectroscopy (XPS) was employed to elucidate the incorporation of Ti^{4+} dopants from TiO_2 underlayer into α–Fe_2O_3 nanostructures when sintered at 800°C. From the survey scan of XPS, some Ti peaks were observed for the 800°C sintered samples, as shown in Fig. 3a. The 550°C sample does not show any Ti within the detection limit from the surface of the α–Fe_2O_3 photoanodes, while the 800°C samples showed distinct peaks at 457.9 and 463.7 eV, confirming the presence of Ti^{4+} ions in the α–Fe_2O_3 nanostructures.[21, 22]

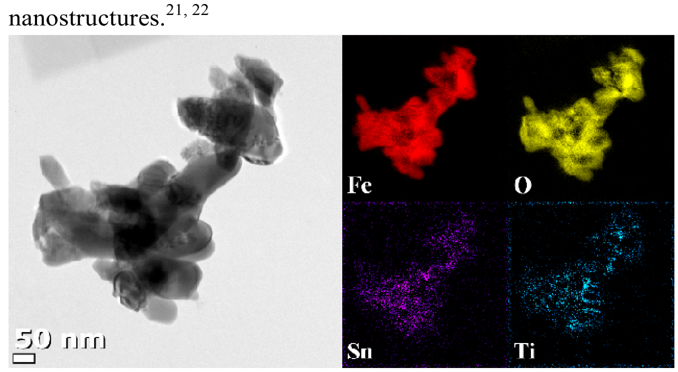

Fig. 4. Typical low-magnification TEM image of FTO/TiO_2/α–Fe_2O_3 photoanodes annealed at 800°C, and its respective elemental mapping images from EELS analysis.

Additional Sn peaks can also be observed for both 550°C and 800°C sintered photoanodes. Sn peaks originated from Sn diffusion from the FTO substrate. When sintered at 800°C, Sn from the FTO substrates is fortuitously doped into the α–Fe_2O_3 photoanodes,[23, 24] a similar intentional Ti^{4+} doping is observed for 800°C sintered FTO/TiO_2/α–Fe_2O_3 photoanodes, however further research is needed to confirm this explanation. The elemental mapping images (Fig. 4) show that both the elemental Sn and Ti were uniformly distributed over the α–Fe_2O_3 nanorods. The Ti distribution may not be perfectly uniform, but it's distributed over the entire nanorod morphology.

Fig. 5 (a) depicts the photocurrent response of FTO/α–Fe_2O_3 and FTO/TiO_2/α–Fe_2O_3 photoanodes sintered at 550 and 800°C in the dark and under illumination. The concentration of the TiO_2 sol determines the thickness of the TiO_2 thin film formed on the surface of the FTO substrates. Based on ellipsometric measurements, the thicknesses of the TiO_2 underlayers for 5 to 25 mM sol concentrations were found to be between 5 and 9 nm, respectively.

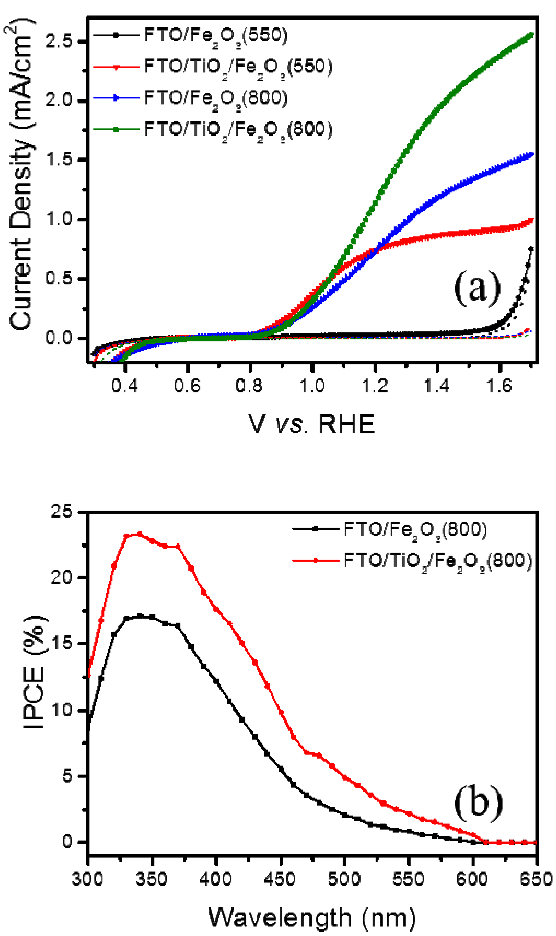

Fig. 5. (a) Photocurrent density-potential (*J-V*) curves for PEC water oxidation reaction sintered at 550 and 800°C and (b) IPCE spectra of FTO/α–Fe_2O_3 and FTO/TiO_2/α–Fe_2O_3 photoanodes sintered at 800°C using 1 M NaOH under 1 sun standard illumination conditions.

Further, the photocurrent increased with increasing TiO_2 sol concentration up to 10 mM, as shown in Figs. S4 and S5 †. At lower TiO_2 sol concentrations, the surface of the FTO substrate was not fully covered, leaving islands of TiO_2. However, a higher concentration resulted in thicker TiO_2 films, a decrease in photocurrent, and an anodic shift of the photocurrent onset potential (Fig. S4 †).[12] Previously observed photo-activity of 550°C sintered hematite nanorods on FTO substrates without a TiO_2 underlayer was poor (0.029 mA/cm^2 at 1.23 V *vs*. RHE).[18] However, hematite nanorods with a TiO_2 underlayer sintered at 550°C showed a relatively larger photocurrent of 0.77 mA/cm^2 at 1.23 V *vs*. RHE. Sivula et al.[23] reported that a high temperature sintering process (800°C) called "activation of hematite" is required to enhance the photo-activity of pristine hematite photoanodes. At a 10 mM TiO_2 sol concentration, the FTO/TiO_2/α–Fe_2O_3 photoanodes showed a much higher photocurrent of 1.28 mA/cm^2 compared to that of FTO/α–Fe_2O_3 photoanodes of 0.8 mA/cm^2 at 1.23 V *vs*. RHE, respectively (Fig. S5 †).

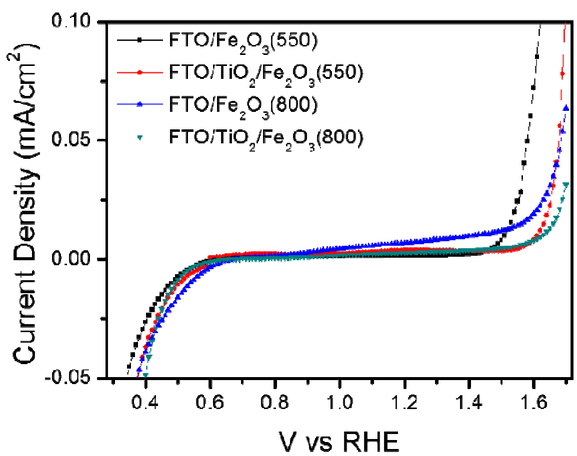

Fig. 6. Photocurrent-potential (*J-V*) curves for PEC water oxidation reaction of FTO/α–Fe_2O_3 and FTO/TiO_2/α–Fe_2O_3 photoanodes annealed at 550 and 800°C under dark conditions.

For 550°C sintered FTO/TiO2/α–Fe_2O_3 photoanodes, the improved photocurrent could be due to the suppression of electron back injection from FTO to hematite photoanode leading to better charge collection and higher photocurrent.[9] TiO_2 underlayer acts as a barrier layer preventing the electron recombination at the FTO/ α–Fe_2O_3 interface, as TiO_2 has a large conduction band compared to FTO or hematite.[25] It is assumed that the better interfacial properties and the blocking layer effect of FTO/TiO_2/α–Fe_2O_3 photoanodes enhances electron transport and charge collection.[26,27] However, the exact nature of the underlayers for improved PEC performance is still unclear and needs further detailed studies. On the other hand, for FTO/TiO_2/α–Fe_2O_3 photoanodes sintered at 800°C, enhanced electron transport properties due to Ti^{4+} doping is highly probable. A similar fortuitous doping is highly probable when FTO/TiO_2/α–Fe_2O_3 photoanodes were sintered at 800°C for hematite activation.[28,29] From Fig. 6, a decrease in dark current is observed for 550 and 800°C sintered FTO/TiO_2/α–Fe_2O_3 photoanodes compared to FTO/α–Fe_2O_3 photoanodes at similar sintering conditions. Such variation in dark current may be attributed to improvements in electron transport properties at the FTO/TiO_2/α–Fe_2O_3 interface by blocking the electron back transfer from hematite to the FTO conducting substrates.[26]

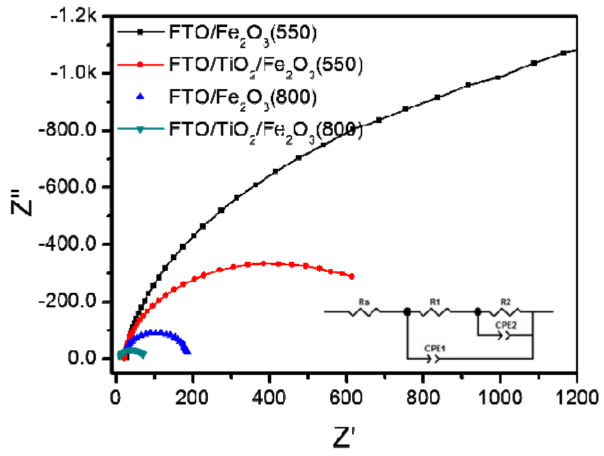

Fig. 7. Nyquist plots of FTO/α–Fe_2O_3 and FTO/TiO_2/α–Fe_2O_3 photoanodes sintered at 550 and 800°C using 1 M NaOH under 1-sun illumination conditions. The inset of the Nyquist plot represents the equivalent circuit for EIS.

Additional incident photon-to-current-efficiency (IPCE) measurements were carried out for 800°C sintered FTO/α–Fe_2O_3 and FTO/TiO_2/α–Fe_2O_3 photoanodes, as shown in Fig. 5b, to evaluate the spectral response for water splitting between 300 to 650 nm at 1.4 V RHE. In comparison to FTO/α–Fe_2O_3, the FTO/TiO_2/α–Fe_2O_3 photoanodes showed higher IPCE values in the whole visible spectrum, indicating higher quantum yield for TiO_2 underlayer samples. Further, the FTO/TiO_2/α–Fe_2O_3 photoanodes demonstrate an IPCE as high as 23.3% at 340 nm for 1.4 V *vs*. RHE. This IPCE result indicates a positive effect of TiO_2 underlayers on water splitting efficiency.

Table 1. Output of the Equivalent Circuit Model for the FTO/α–Fe_2O_3 and FTO/TiO_2/α–Fe_2O_3 photoanodes annealed at 550 and 800°C using 1M NaOH, under 1 sun standard illumination conditions from the Nyquist plot.

(R/Ω) (CPE/F)	FTO/α-Fe_2O_3 (550°C)	FTO/TiO_2/α-Fe_2O_3 (550°C)	FTO/α-Fe_2O_3 (800°C)	FTO/TiO_2/α-Fe_2O_3 (800°C)
R_S	28.3	14.1	39.5	24.2
R_{CT1}	516	19.1	98.1	59.2
CPE_1	1.03×10^{-7}	7.21×10^{-6}	1.39×10^{-5}	1.86×10^{-5}
R_{CT2}	5978	991.2	113.3	45.2
CPE_2	5.28×10^{-6}	9.35×10^{-5}	2.72×10^{-5}	3.55×10^{-5}

Using electrochemical impedance spectroscopy (EIS), the charge transport kinetics and the interfacial properties of both 550 and 800°C sintered FTO/α–Fe_2O_3 and FTO/TiO_2/α–Fe_2O_3 photoanodes were studied. The improvement in electrical contact between the FTO substrate and hematite nanostructure can be experimentally deduced from the EIS measurement.[30] All EIS spectra were fitted using ZView software with the equivalent circuit shown in Fig. 7. In brief, from Table 1 (Fig. S6 †), the sheet resistance (R_S) is reduced from 29 to 15 Ω for 550°C and 40 to 25 Ω for 800°C sintered photoanodes. A lower R_S indicates that the conductivity of FTO/TiO_2/α–Fe_2O_3 is higher compared to that of the FTO/α–Fe_2O_3 photoanodes. The charge transport resistance at the FTO/TiO_2 interface (R_{CT1}) decreased with the TiO_2 underlayer from 516 to 39 Ω for 550°C and 98 to 59 Ω for 800°C sintered photoanodes, while charge transport resistance of the α–Fe_2O_3 and the α–Fe_2O_3/electrolyte interface (R_{CT2}) decreased from 5978 to 991 Ω for 550°C and 113 to 45 Ω for 800°C sintered photoanodes for FTO/TiO_2/α–Fe_2O_3, respectively. The charge transport resistance value (R_{CT1}) was drastically reduced after introducing the TiO_2 underlayer (for both 550 and 800°C sintering), suggesting that the interfacial resistance at the FTO/α–Fe_2O_3 interface was significantly reduced. This decrease in R_{CT1} could be attributed to improved adhesion between the hematite nanostructures and FTO substrate by incorporating a TiO_2 underlayer and reduced electron-charge recombination via effective charge collection. A dramatic decrease in R_{CT2} was observed for 800°C sintered FTO/TiO_2/α–Fe_2O_3 photoanodes compared to 550°C sintered FTO/TiO_2/α–Fe_2O_3 photoanodes, indicating that there is an increase in the number of charge carriers with Sn diffusion into the hematite lattice for 800°C sintered FTO/α–Fe_2O_3 photoanodes. Further, elimination of the dead layer at the FTO/α–Fe_2O_3 interface occurs as a result of Ti^{4+} doping for FTO/TiO_2/α–Fe_2O_3 photoanodes. Fortuitous doping of Sn from FTO into hematite lattice observed during the activation step,[23,24] is successfully converted into an intentional doping of Ti^{4+} from the TiO_2 underlayer into the hematite lattice, which is highly probable at 800°C sintering conditions.

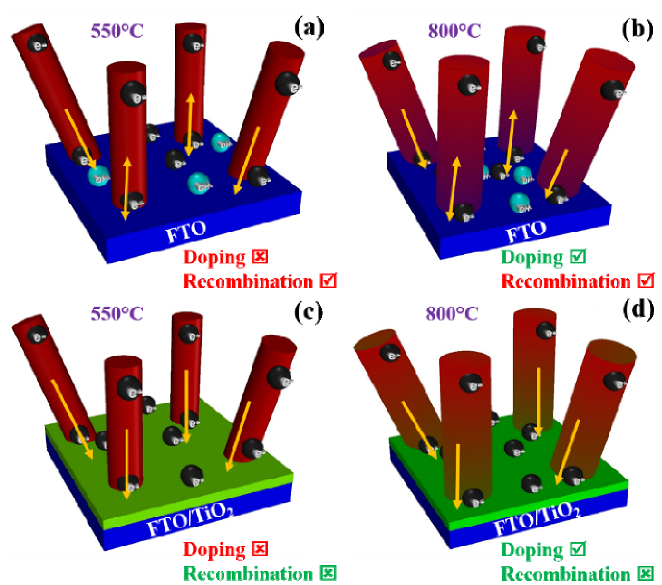

Scheme 1. Schematic representation of TiO_2 underlayer effect on hematite photoanodes. (a) and (b) FTO/ α–Fe_2O_3 sintered at 550 and 800°C, (c) and (d) FTO/TiO_2/α–Fe_2O_3 sintered at 550 and 800°C, respectively.

In addition, a higher Debye-Waller factor was observed for 800°C sintered FTO/TiO_2/α–Fe_2O_3 photoanodes, the most probable cause might be the presence of structural disordering with Ti^{4+} doping due to introduction of an interfacial TiO_2 underlayer. Thus, both the suppression of electron back injection from FTO to the hematite and interfacial doping of Ti^{4+} during high temperature sintering seem to be likely reasons for improved performance of the TiO_2 underlayer photoanodes, while only suppression of electron back injection from FTO to hematite for 550°C sintered FTO/TiO_2/α–Fe_2O_3 photoanodes occurs, as explained in Scheme 1. In order to investigate whether there is a similar effect on surface treated FTO/α–Fe_2O_3 photoanodes, we compared the surface treated samples with bare FTO/α–Fe_2O_3 photoanodes, as shown in Fig. S7 †. We observed a mild increase in photocurrent as well as an undesired anodic shift in the onset potential of Ti-doped FTO/α–Fe_2O_3 photoanodes. Thus, the TiO_2 underlayer effect is far superior to that of TiO_2 surface treated FTO/α–Fe_2O_3 photoanodes.

Conclusions

In summary, simple spin coating was used to prepare thin, compact TiO_2 blocking layers on FTO substrates as an alternative to the complex ALD method. By varying the TiO_2 sol concentration, we optimized the TiO_2 compact layers for use as underlayers. We also conclude that the TiO_2 underlayer significantly alters the morphology of hematite 1-D nanostructures. Fortuitous doping of Sn from FTO into hematite lattice during the activation step, is successfully converted into intentional doping of Ti^{4+} from the TiO_2 underlayer into the hematite lattice has been confirmed by XPS measurements. We showed that the TiO_2 underlayer dramatically enhances the PEC water oxidation performance. This performance enhancement was a combination of improved interfacial properties (FTO/TiO_2/α–Fe_2O_3) and intentional Ti^{4+} doping into α–Fe_2O_3 apart from Sn diffusion from FTO substrates at high temperature, while only improved interfacial properties (FTO/TiO_2/α–Fe_2O_3) at low temperature sintering conditions. These improvements result in excellent charge transport and collection efficiency. This the first report on the effect of TiO_2 underlayers for thicker hematite nanorods rather than the ultrathin hematite photoanodes widely used.

Acknowledgements

This research was supported by the Basic Science Research Programs through the National Research Foundation of Korea (NRF) funded by the Ministry of Education, Science and Technology (2012R1A6A3A04038530), and by research funds of Chonbuk National University in 2014.

Notes and references

[a] Division of Biotechnology, Advanced Institute of Environmental and Bioscience, College of Environmental and Bioresource Sciences, Chonbuk National University, Iksan 570-752, Republic of Korea

[b] School of Energy and Chemical Engineering, Ulsan National Institute of Science and Technology, 50 UNIST-gil, Ulsan 689-798, Republic of Korea

[c] Pohang Accelerator Laboratory (PAL), Pohang University of Science and Technology
(POSTECH), Pohang 790–784, Republic of Korea

* Corresponding author. E-mail address: jangjs75@jbnu.ac.kr

† Electronic Supplementary Information (ESI) available: [Detailed characterization of TiO_2 underlayers (XRD, UV and TEM-EDS) and TiO_2 underlayer optimization for PEC cells]. See DOI: 10.1039/c000000x/

1. A. Fujishima and K. Honda, *Nature*, 1972, 238, 37-38.
2. M. Gratzel, *Nature*, 2001, 414, 338-344.
3. P. S. Bassi, Gurudayal, L. H. Wong and J. Barber, *Phys Chem Chem Phys*, 2014, 16, 11834-11842.
4. Z. S. Li, W. J. Luo, M. L. Zhang, J. Y. Feng and Z. G. Zou, *Energ Environ Sci*, 2013, 6, 347-370.
5. C. Liu, N. P. Dasgupta and P. D. Yang, *Chem Mater*, 2014, 26, 415-422.
6. K. Sivula, F. Le Formal and M. Gratzel, *Chemsuschem*, 2011, 4, 432-449.
7. X. Lu, S. Xie, H. Yang, Y. Tong and H. Ji, *Chemical Society Reviews*, 2014, DOI: 10.1039/C3CS60392J.
8. O. Zandi, B. M. Klahr and T. W. Hamann, *Energ Environ Sci*, 2013, 6, 634-642.
9. T. Hisatomi, H. Dotan, M. Stefik, K. Sivula, A. Rothschild, M. Gratzel and N. Mathews, *Adv Mater*, 2012, 24, 2699-2702.
10. F. Le Formal, M. Gratzel and K. Sivula, *Adv Funct Mater*, 2010, 20, 1099-1107.
11. E. Palomares, J. N. Clifford, S. A. Haque, T. Lutz and J. R. Durrant, *J Am Chem Soc*, 2003, 125, 475-482.
12. T. Hisatomi, J. Brillet, M. Cornuz, F. Le Formal, N. Tetreault, K. Sivula and M. Gratzel, *Faraday Discuss*, 2012, 155, 223-232.
13. C. K. Ong, S. Dennison, S. Fearn, K. Hellgardt and G. H. Kelsall, *Electrochim Acta*, 2014, 125, 266-274.
14. D. G. Wang, Y. Y. Zhang, J. Q. Wang, C. Peng, Q. Huang, S. Su, L. H. Wang, W. Huang and C. H. Fan, *Acs Appl Mater Inter*, 2014, 6, 36-40.
15. P. Lellig, M. A. Niedermeier, M. Rawolle, M. Meister, F. Laquai, P. Muller-Buschbaum and J. S. Gutmann, *Phys Chem Chem Phys*, 2012, 14, 1607-1613.
16. L. Vayssieres, N. Beermann, S. E. Lindquist and A. Hagfeldt, *Chem Mater*, 2001, 13, 233-235.
17. B. Ravel and M. Newville, *J Synchrotron Radiat*, 2005, 12, 537-541.
18. J. Y. Kim, G. Magesh, D. H. Youn, J. W. Jang, J. Kubota, K. Domen and J. S. Lee, *Sci Rep-Uk*, 2013, 3, 2681.
19. D. Bersani, P. P. Lottici and A. Montenero, *J Raman Spectrosc*, 1999, 30, 355-360.
20. S. H. Shen, C. X. Kronawitter, D. A. Wheeler, P. H. Guo, S. A. Lindley, J. G. Jiang, J. Z. Zhang, L. J. Guo and S. S. Mao, *J Mater Chem A*, 2013, 1, 14498-14506.
21. M. Rioult, H. Magnan, D. Stanescu and A. Barbier, *J Phys Chem C*, 2014, 118, 3007-3014.
22. N. Mirbagheri, D. G. Wang, C. Peng, J. Q. Wang, Q. Huang, C. H. Fan and E. E. Ferapontova, *Acs Catal*, 2014, 4, 2006-2015.
23. K. Sivula, R. Zboril, F. Le Formal, R. Robert, A. Weidenkaff, J. Tucek, J. Frydrych and M. Gratzel, *J Am Chem Soc*, 2010, 132, 7436-7444.
24. Y. C. Ling, G. M. Wang, D. A. Wheeler, J. Z. Zhang and Y. Li, *Nano Lett*, 2011, 11, 2119-2125.
25. D. Wang, X. T. Zhang, P. P. Sun, S. Lu, L. L. Wang, Y. A. Wei and Y. C. Liu, *International Journal of Hydrogen Energy*, 2014, 39, 16212-16219.
26. X. J. Shi, K. Zhang and J. H. Park, *International Journal of Hydrogen Energy*, 2013, 38, 12725-12732.
27. S. Ito, P. Liska, P. Comte, R. Charvet, P. Pechy, U. Bach, L. Schmidt-Mende, S. M. Zakeeruddin, A. Kay, M. K. Nazeeruddin

and M. Gratzel, *Chemical Communications*, 2005, DOI: 10.1039/B505718C, 4351-4353.
28. R. Franking, L. S. Li, M. A. Lukowski, F. Meng, Y. Z. Tan, R. J. Hamers and S. Jin, *Energ Environ Sci*, 2013, 6, 500-512.
29. L. Wang, C. Y. Lee and P. Schmuki, *Electrochem Commun*, 2013, 30, 21-25.
30. T. Lopes, L. Andrade, H. A. Ribeiro and A. Mendes, *International Journal of Hydrogen Energy*, 2010, 35, 11601-11608.

Graphical Table of Contents

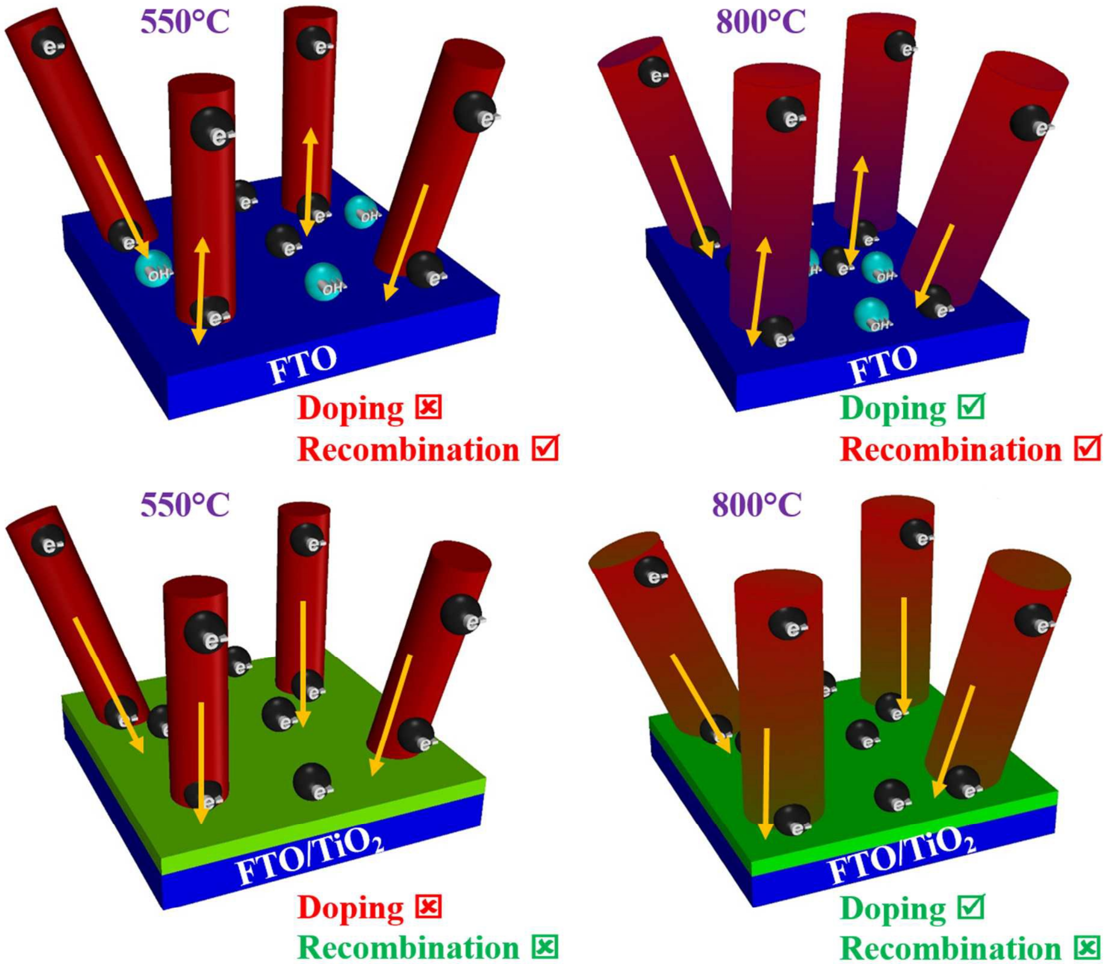

The TiO_2 underlayer effectively suppresses charge recombination at the FTO/α–Fe_2O_3 interface and allows Ti^{4+} doping apart from Sn diffusion from FTO substrates when sintered at high temperatures (800°C), thus enhancing the charge transport and collection while only charge recombination is suppressed at lower sintering temperatures (550°C).